Journal of Power Sources 182 (2008) 307–316

Contents lists available at ScienceDirect

Journal of Power Sources

journal homepage: www.elsevier.com/locate/jpowsour

CO-PrOx reactor design by model-based optimization

Diego G. Oliva, Javier A. Francesconi, Miguel C. Mussati, Pio A. Aguirre*

INGAR Instituto de Desarrollo y Diseño (CONICET-UTN), Avellaneda 3657, CP: S3002GJC, Santa Fe, Argentina

ARTICLE INFO

Article history:
Received 15 January 2008
Received in revised form 3 March 2008
Accepted 4 March 2008
Available online 25 March 2008

Keywords:
CO-PrOx
Reactor design
Optimization
Fuel cell

ABSTRACT

This work analyzes the CO-PrOx reactor design as a component of the CO clean-up system of the ethanol processor for H_2 production applied to PEM fuel cells. The operating conditions of the processor require compact and lightweight pieces of equipment and efficient operation at different conditions. An egg-shell catalyst type of Pt/Al_2O_3 is considered. One-dimensional heterogeneous catalytic reactor model accounting for interfacial gradients is used to optimize the PrOx reactor. Different reactor components are added gradually to illustrate how the system dimensions and configuration change after optimization. The optimization problem determines the optimal reactor length, reactor diameter, catalyst particle diameter, inlet reactants temperature and insulating material thickness that minimize the total system volume. On these model-based results, the final reactor design is mainly governed by the presence of hemispherical heads (distributor and collector). Different inlet CO compositions and power generation targets are analyzed. According to the inlet CO level, more than one catalytic stage is required to meet design goals and fulfill process constraints. The model-based reactor optimization of the pseudo-adiabatic operation allows obtaining both designs for reducing volumes and optimal operating conditions that allows conventional reactor technology. Afterwards, simulation runs based on a rigorous one-dimensional heterogeneous catalytic reactor model accounting for intra-particle gradients are performed using data obtained from model-based optimization results. The aim of these simulations is to verify feasibility of the optimal design obtained from the proposed one-dimensional heterogeneous catalytic reactor model without intra-particle gradients, which is intended to approximate an egg-shell catalyst behavior. The present work reflects clearly the advantages of applying mathematical programming techniques to optimize both design and operation conditions of the PrOx reactor.

1. Introduction

During the last decade, there have been important advances in fuel cells technology. Fuel cells are being developed for applications to electrical energy generation and co-generation systems (coupled heat and power) in both stationary and mobile systems. Since fuel cells are high-efficiency energy converter devices and because of their low polluting emission levels, they become more and more attractive as a power generation alternative, specially in the transportation industry [1,2].

Proton exchange membrane fuel cell (PEMFC) demands a free-CO hydrogen stream for operation. Since CO is adsorbed on the catalyst surface causing catalyst poisoning, it is necessary to reach CO concentrations of less than 10 ppm for preventing irreversible damage and to facilitate the electrochemical reaction on the Pt electrode. The conditioning of the gas stream generated from the steam reforming of ethanol is partially performed by the water–gas-shift reaction (WGS). The WGS stage in the reforming systems allows achieving an outlet gas composition with a typical CO composition of 0.5–2% (v/v). Afterwards, a final CO reduction is needed.

Physical methods (pressure swing adsorption (PSA)) and catalytic methods (methanation and preferential oxidation) have been studied for selective CO removal from a hydrogen-rich stream. Among these different hydrogen purification systems the CO preferential oxidation is preferred for small-scale reforming systems because of its relative simple implementation, lower operating costs and minimal hydrogen loss [3,4].

For fuel cell applications, a compact, efficient and reliable fuel processor is desirable. Process synthesis and design tasks are similar to other industrial reforming processes. However, the production capacity level required by fuel processors for vehicles or other similar devices is lower when compared to industrial processes. Thus, process units of small size and specific designs are required.

* Corresponding author. Tel.: +54 342 453 4451; fax: +54 342 455 3439.
E-mail address: paguir@santafe-conicet.gov.ar (P.A. Aguirre).

0378-7753/$ – see front matter © 2008 Elsevier B.V. All rights reserved.
doi:10.1016/j.jpowsour.2008.03.043

Nomenclature

a_v	external catalyst surface area per unitary reactor volume (cm^{-1})
A_r	cross-reactor area (cm^2)
C_i	component concentration along the reactor ($mol\,cm^{-3}$)
C_{p_f}	heat capacity ($J\,g^{-1}\,K^{-1}$)
$C_{S,i}$	component concentration inside the catalyst pore ($mol\,cm^{-3}$)
$C^S_{S,i}$	component concentration at the external catalyst surface ($mol\,cm^{-3}$)
$D_{i,k}$	binary diffusion ($cm^2\,s^{-1}$)
D_p	catalyst particle diameter (cm)
D_t	reactor tube diameter (cm)
$Dif_{i,m}$	diffusion coefficient of the component i in the gas mixture ($cm^2\,s^{-1}$)
e_{ins}	insulating material thickness (cm)
e_t	reactor tube thickness (cm)
F_i	molar flow of component i ($mol\,s^{-1}$)
G	mass flow per unitary reactor area ($g\,cm^{-2}\,s^{-1}$)
h_f	energy transfer coefficient in the film ($J\,cm^{-2}\,s^{-1}\,K^{-1}$)
ΔH_j	heat of reaction ($J\,mol^{-1}$)
$k_{g,i}$	mass transfer coefficient in the film ($cm\,s^{-1}$)
L_t	reactor length (cm)
M_i	molecular weight of component i ($g\,mol^{-1}$)
P	pressure (atm)
Q^{ex}	heat exchanged between the reactor and its surroundings
r_j	reaction rate ($mol\,g\text{-}cat^{-1}\,s^{-1}$)
T_f	fluid temperature (K)
T_{ins}	surface insulating material temperature (K)
T_s	temperature inside the catalyst pore (K)
T^S_S	temperature at the catalyst surface (K)
Tc_1	critical temperature of the i component (K)
V_{total}	volume (cm^3)
Vc_i	critical volume of the component i ($cm^3\,mol^{-1}$)

Greek letters

α^i_j	stoichiometric coefficient of component i in reaction j
ε_b	bed porosity
λ_f	gas thermal conductivity ($J\,cm^{-1}\,s^{-1}\,K^{-1}$)
μ_f	gas viscosity ($g\,cm^{-1}\,s^{-1}$)
ρ_b	bulk catalyst density ($g\text{-}cat\,cm^{-3}$)
ρ_f	gas phase density ($g\,cm^{-3}$)
ρ_p	catalyst density ($g\text{-}cat\,cm^{-3}$)

The aim of this work is focused on investigating the PrOx reactor as a process component of a fuel processor for applications in PEM-type fuel cells, and showing how the reactor design using mathematical programming techniques allows computing both reduced volumes and optimal operation conditions. Different reactor configurations, reactor size and relative sizes of the reactor components (insulating material, reactor tube and reactive bed) can be evaluated; moreover, process performance bottlenecks and opportunities for optimization can be identified and analyzed. This knowledge can be used for process improvements such as lower unit weight and costs, and higher global efficiency.

2. Preferential oxidation of carbon monoxide

Carbon monoxide oxidation to obtain carbon dioxide in a hydrogen-rich stream was first investigated in the ammonia industry in the 60s. As a result of those former works, a highly active and selective platinum-based catalyst – named Selectoxo – was developed [3]. The main reactions involved are: carbon monoxide oxidation (1) and hydrogen oxidation (2):

$$CO + \tfrac{1}{2}O_2 \rightarrow CO_2 \quad \Delta H^0_{298} = -283.2\,kJ\,mol^{-1} \quad \text{desirable} \qquad (1)$$

$$H_2 + \tfrac{1}{2}O_2 \rightarrow H_2O \quad \Delta H^0_{298} = -241\,kJ\,mol^{-1} \quad \text{undesirable} \qquad (2)$$

Some researchers pointed out that, depending on the operation conditions and the catalyst used, the inverse water–gas-shift reaction rWGS (3) and the methanation reaction (4) can also occur, but to a lower extent [4,5].

$$CO + H_2O \leftrightarrow CO_2 + H_2 \quad \Delta H^0_{298} = -42.2\,kJ\,mol^{-1} \qquad (3)$$

$$CO + 3H_2 \leftrightarrow CH_4 + H_2O \quad \Delta H^0_{298} = -205.3\,kJ\,mol^{-1} \qquad (4)$$

Excessive hydrogen consumption is undesirable since the system efficiency diminishes, and makes it difficult to control the system temperature. Thus, the catalyst has to facilitate or favor reaction (1) over reaction (2) [6]. The catalyst would ideally have to selectively oxidize about 10,000 ppm (1%) CO to less than 5 ppm without oxidizing any of the present 30–70% H_2. For example, for a molar ratio $O_2/CO = 2$ and using a Pt/alumina-based catalyst, a 100 ppm CO concentration is obtained at the reactor outlet. However, using the same catalyst and for a O_2/CO ratio equal to 3, the CO removal is complete in a mixture containing 1% CO. But the O_2 excess also consumes H_2, consequently decreasing the processor efficiency. In addition, if a large excess of air is supplied, the temperature control becomes difficult due to the exothermic nature of the reaction [7]. Then, it is necessary to have a highly selective catalyst that allows operating at O_2 levels close to the stoichiometric one. The selection of a highly selective catalyst, reactor design and determination of operation conditions are critical aspects that have to be addressed. Once the catalyst to be used is defined, temperature, O_2/CO ratio, reactor operation mode and the number of stages (i.e. reactors in-series) constitute key decisions, leading to opportunities for process optimization.

The efforts for improving the PrOx reactor performance have been focused in a wide spectrum of subjects, including the development of more active catalysts [3,5,6,8–15], experimental and theoretical studies to formulate kinetic expressions for novel catalysts [8,12,15–18] and theoretical studies related to the effect of heat transfer resistance on PrOx reaction behavior [16]. Research is also concerned with applying and evaluating non-conventional reactors such as microreactors [17] and monolith reactors [18].

Several catalysts have been formulated to perform the carbon monoxide preferential oxidation, most of them based on noble metals. Researchers have reported the use of supported catalysts based on iridium (Ir) [3], palladium (Pd) [3], platinum (Pt) [3,5,6,8,9], gold (Au) [8,10], rhodium (Rh) [3], rutenium (Ru) [3,11,12] and platinum-based alloys [3].

In order to reduce costs and improve selectivity, recent works have been focused on using non-noble metals. Sedmak et al. [13] developed a nanostructured non-stoichiometric $Cu_{0.1}Ce_{0.9}O_2$-Y catalyst. Zhou et al. [14] investigated the catalytic properties of Ni, Co and Co–Ni supported on activated carbon. Mariño et al. reported that the catalytic system CuO–CeO_2 is very active and selective for CO oxidation in the presence of a large amount of H_2 [15]. These metals have demonstrated to have a high activity for CO oxidation in hydrogen-rich streams.

Platinum-based catalysts, supported on alumina or silica are the most used and investigated as conventional catalysts for the CO preferential oxidation. Although the oxidation rate of H_2 is several magnitude orders higher than CO on a Pt surface, and that its concentration in the gaseous stream entering the reactor is two magnitude orders greater than CO, the preferential oxidation of CO is possible due to the relative values of the adsorption heats of the substances involved on a Pt surface [19]. Therefore, all these catalytic systems exhibit a range or "window" of operation temperature. Whereas on the one hand sufficiently high operation temperatures are desirable to increase the reaction rate (1) and to diminish consequently the reactor size, on the other hand it is convenient to operate at sufficiently low temperatures to avoid H_2 oxidation. The temperature range in which activity and selectivity requirements are satisfied is so narrow that the catalyst cannot admit small system disturbances. Then, the previously mentioned catalyst types require a precise and complex temperature control system [20].

Zalc and Löffler [21] also pointed out that reactor temperature control is crucial due to the reaction kinetics and the narrow temperature operation range to achieve high selectivity for the desired reaction (1). A single-stage unit operating in adiabatic mode would yield poor system performance. Thus, an optimal reactor design has to include an effective temperature control. To accomplish this, they highlight that the following non-excluding alternatives can be considered: supporting catalyst on a heat exchanger, or using air staged injection or water injection. They also estimated, based on simulations, a catalytic bed volume of approximately 3.5 L for a hydrogen production of around 31 mol min^{-1}, about 5 kg of a catalyst with 0.5% of Pt on γ-alumina in a non-isothermal fixed-bed reactor is needed to reduce CO from 1% mol-basis to less than 50 ppm.

Lee et al. [20] developed a PrOx reactor for a 10 kWe PEMFC using a Pt–Ru/Al_2O_3-based catalyst. In order to diminish the pressure drop and avoid hot spots in the bed, the authors proposed two stage in-series multitubular adiabatic reactors with intermediate cooling. They reported a total system volume about 6280 cm^3, where 1200 cm^3 correspond to the catalyst bed.

Dudfield et al. [22,23] designed, constructed and evaluated a compact unit of a PrOx reactor treating a gaseous stream in a methanol processor for PEMFC used in mobile applications. After evaluating different catalysts, the authors selected a Pt/Ru-based catalyst as it showed higher selectivity and conversion on the studied temperature range [23]. The system design consists of a Pt/Ru-based catalyst supported on the surface of a finned-type heat exchanger using oil as a coolant, arranged in two stages in-series of 0.5 L each. The system reduced the initial CO concentration from 0.5% to less than 20 ppm, operating at an average temperature of 160 °C, and considering the gas flowrate equivalent to produce 5 kWe of electrical power in a PEMFC. For an inlet CO composition of 7000 ppm and a fuel flowrate equivalent to produce 3.75–7.5 kWe, a unique unit of 0.5 L is not enough to reduce the outlet CO level to 20 ppm. Whereas by arranging two reactors in-series of 0.5 L each, it is feasible to achieve a final CO concentration of 10 ppm. By simultaneously increasing the residence time and optimizing the air injection in each stage, an exit CO concentration of 10 ppm is obtained for a flowrate to produce 7.5 kWe in a PEMFC. Based on the same concept, Dudfield et al. [22] developed a reactor to process a stream flowrate equivalent to 20 kWe, where each reactor occupies 2000 cm^3, weighs 2.5 kg and has approximately 1 L available for the reaction with oxygen and 1 L to maintain the temperature by recirculation of a cooling fluid (oil).

Bissett and Oh [18] modeled a monolithic-type reactor operating isothermally and adiabatically.

To the authors' knowledge, model-based optimal reactor design and analysis applying mathematical programming techniques have not been yet addressed in this area. Modeling and optimization allow evaluating which system designs and operation conditions – e.g. adiabatically or isothermally – are more appropriate under different scenarios such as power generation scale, costs structure, fuel cell quality requirements (CO content) and application purposes (mobile or stationary units).

In this paper, a one-dimensional heterogeneous catalytic reactor accounting for interfacial gradients [24] is used to optimize the PrOx reactor. Different reactor components are added gradually to illustrate how the system dimensions and configuration changes after optimization. Different inlet CO compositions and power generation targets are analyzed. After that, simulations with different reactor models will be performed. The aim of these simulations is to verify feasibility of the optimal design obtained with the proposed methodology using the one-dimensional heterogeneous model without intra-particle gradients, which is intended to approximate an egg-shell catalyst behavior.

3. Mathematical model

3.1. Reactor model

In this work, the reactor design is performed based on a one-dimensional heterogeneous model. This model offers higher accuracy for reactor design [25]. The mass and energy balances, and pressure drop along the catalytic bed for the fluid phase and balances for catalyst particles are represented by the following equations [24,26]:

Fluid phase

$$-\frac{dF_i}{dz} = A_r k_{g,i} a_v (C_i - C^S_{S,i}) \tag{5}$$

$$GC_{pr}\frac{dT_f}{dz} = h_f a_v (T^s_s - T_f) - Q^{ex} \tag{6}$$

$$-\frac{dP}{dz} = \frac{G^2}{\rho_f D_p}\frac{1-\varepsilon_b}{\varepsilon_b^3}\left[4.2\left(\frac{1-\varepsilon_b}{Re}\right)^{1/6} + 150\frac{1-\varepsilon_b}{Re}\right] \tag{7}$$

For solid

$$k_{g,i} a_v (C_i - C^S_{S,i}) + \rho_b \sum_{j=1}^{Nrx} \alpha^i_j r_j (C^S_S, T^S_S) = 0 \tag{8}$$

$$h_f a_v (T_f - T^S_S) + \rho_b \sum_{j=1}^{Nrx} (-\Delta H)_j r_j (C^S_S, T^S_S) = 0 \tag{9}$$

Eqs. (5)–(7) represent the mass, energy and momentum balances for the fluid phase with initial conditions at $z = 0$ given by $F_i = F^0_i$, $T_f = T^0_f$ and $P = P^0$. Pressure drop is evaluated using an Ergun-type expression with friction parameters given by Tallmadge correlations [26], which are valid for a wide range of Reynolds numbers ($0.1 < Re/(1-\varepsilon_b) < 10{,}000$). Eqs. (8) and (9) represent the mass and energy balances for the fluid-particle interphase as boundary conditions.

3.2. Physical–chemical parameters and fluid properties

Ideal gas behavior is assumed to evaluate the mixture density of the gas phase (ρ_f). The average molecular weight of the gaseous mixture and the molar flow entering the reactor were used to compute the mass flow per unitary area (G). Correlations for the fluid heat capacity (C_{pr}), viscosity (μ_f) and thermal conductivity (λ_f) are those given in [27].

3.2.1. Viscosity

The Bromley and Wilke modification of the theoretical Hirschfleder method was used to estimate the pure component viscosity [28]:

$$\mu_i = \frac{33.3\sqrt{M_i \mathrm{Tc}_i}}{\mathrm{Vc}_i^{2/3}} \left(1.058 \left(\frac{T_\mathrm{f}}{\mathrm{Tc}_i} \right)^{0.645} - \frac{0.261}{(1.9(T_\mathrm{f}/\mathrm{Tc}_i))^{0.9 \log_{10}(1.9(T_\mathrm{f}/\mathrm{Tc}_i))}} \right) \quad (10)$$

The gas mixture viscosity was calculated from Wilkeĭs method [27].

$$\mu_\mathrm{f} = 1.00\mathrm{E}-06 \sum_i \left[y_i \mu_i \left(\sum_j y_j \varphi_{ij} \right)^{-1} \right] \quad (11)$$

where $\varphi_{ij} \cong \varphi_{ji}^{-1} = (M_j M_i^{-1})^{1/2}$ as given by Herning and Zipperer (see Reid et al. [27])

3.2.2. Thermal conductivity

The pure component thermal conductivities were calculated using the Eucken's approximation [28]:

$$\lambda_i = \mu_i 4.1890 \times 10^{-4} \left(C_{p_i} 2.394 \times 10^{-4} + \frac{2.48}{M_i} \right) \quad (12)$$

The following expression was used for computing the mixture thermal conductivity [28,29]:

$$\lambda_\mathrm{f} = 0.01 \frac{\sum_i y_i \lambda_i M_i^{1/3}}{\sum_i y_i M_i^{1/3}} \quad (13)$$

3.2.3. Heat capacity

The fluid mass heat capacity is calculated as $C_{p_f} = \sum_i M_i y_i C_{p_i} / \sum_i M_i y_i$, where the pure component heat capacities (C_{p_i}) were obtained from Prausnitz and co-workers [27].

3.2.4. Mass and energy transfer coefficients

The frequently used correlation for the mass and energy transfer coefficients in the film, proposed by Petrovic and Thodos for $3 < Re < 2000$ (see Satterfield [30]), is here used.

$$\frac{k_{\mathrm{g},i} D_\mathrm{p} \varepsilon_\mathrm{b}}{\mathrm{Dif}_{i,\mathrm{m}}} = 0.357 Re^{0.641} \left(\frac{\mu_\mathrm{f}}{\rho_\mathrm{f} \mathrm{Dif}_{i,\mathrm{m}}} \right)^{1/3} \quad (14)$$

$$\frac{h_\mathrm{f} \varepsilon_\mathrm{b}}{G C_{p_\mathrm{f}}} = 0.357 \left(\frac{D_\mathrm{p} G}{\mu_\mathrm{f}} \right)^{-0.359} \left(\frac{C_{p_\mathrm{f}} \mu_\mathrm{f}}{\lambda_\mathrm{f}} \right)^{-2/3} \quad (15)$$

$\mathrm{Dif}_{i,\mathrm{m}}$ is the diffusion coefficient of component i in the gas mixture, and is calculated according to the Wilke equation:

$$\frac{1}{\mathrm{Dif}_{i,\mathrm{m}}} = \sum_{k \neq i} \frac{y_i}{D_{i,k}} \quad (16)$$

The binary diffusion coefficients $D_{i,k}$ are given as a function of the diffusion volumes by the Fuller et al. estimation (see Reid et al. [27]):

$$D_{i,k} = \frac{0.0014489475\, T_\mathrm{f}^{1.75} (1/M_i + 1/M_k)^{1/2}}{P\sqrt{2}[(\Sigma_\mathrm{v})_i^{1/3} + (\Sigma_\mathrm{v})_k^{1/3}]^2} \quad (17)$$

3.2.5. Bed properties

The bed porosity (ε_b) is estimated by the Haughey and Beveridge expression given by Froment and Bischoff [24]:

$$\varepsilon_\mathrm{b} = 0.38 + 0.073 \left[1 - \frac{(D_\mathrm{t}/D_\mathrm{p} - 2)^2}{(D_\mathrm{t}/D_\mathrm{p})^2} \right] \quad (18)$$

For spherical shape particles, the external catalyst surface area per unitary reactor volume (a_v) is computed by $a_\mathrm{v} = 6(1 - \varepsilon_\mathrm{b})/D_\mathrm{p}$. The mass of catalyst per unitary bed volume (ρ_b) is calculated according to $\rho_\mathrm{b} = \rho_\mathrm{p}(1 - \varepsilon_\mathrm{b})$.

3.3. Insulation model

In Eq. (6), Q^ex is the heat exchanged between the reaction system and its surroundings. Q^ex represents the heat flow per unitary reactor bed volume, and is related to the fluid temperature and the tube wall temperature by the heat transfer coefficient (h_w) computed by the Leva correlation [24].

$$Q^\mathrm{ex} = \frac{4}{D_\mathrm{t}} h_\mathrm{w} (T_\mathrm{f} - T_\mathrm{w}) \quad (19)$$

In the adiabatic operation mode $Q^\mathrm{ex} = 0$. In the thermally insulated reactor case, a heat loss towards the surroundings is considered by modeling the energy transfer by heat conduction through the tube and insulation materials, and by convection and radiation from the insulation surface to the environment. By applying the Fourier law to a cylindrical geometry, and considering temperature dependence of the thermal conductivity, the heat flow by conduction through the insulation material results in the following expression:

$$Q^\mathrm{ex} = \frac{8}{D_\mathrm{t}^2 \, ln(D_\mathrm{ins}/D_\mathrm{t})} \int_{T_\mathrm{ins}}^{T_\mathrm{w}} k(T) \mathrm{d}T \quad (20)$$

Finally, the heat flow is related to the heat loss from insulation surface [31] by convection and radiation by Eqs. (22) and (23), respectively.

$$Q^\mathrm{ex} = \frac{4 D_\mathrm{ins}}{D_\mathrm{t}^2} (q_\mathrm{cv} + q_\mathrm{rad}) \quad (21)$$

$$q_\mathrm{cv} = 2.3613 \times 10^{-4} \left(\frac{1}{D_\mathrm{ins}} \right)^{0.2} \left(\frac{1}{(T_\mathrm{amb} + T_\mathrm{ins}) 0.9 - 459.67} \right)^{0.181} \times (T_\mathrm{ins} - T_\mathrm{amb})^{1.266} \quad (22)$$

$$q_\mathrm{rad} = \sigma \varepsilon_\mathrm{ins} ((T_\mathrm{ins})^4 - (T_\mathrm{amb})^4) \quad (23)$$

3.4. Kinetics aspects

In spite of the large number of works proposing kinetic expressions for the CO oxidation, only a few consider simultaneously the H_2 oxidation. Other works report expressions for the H_2 oxidation over platinum separately [12,15–18]. Choi and Stenger [5] derived kinetic expressions for the simultaneous oxidation of CO and H_2 and the water–gas-shift reaction obtained over a Pt–Fe/Al_2O_3-based catalyst. As small numerical values are computed for the partial pressure of the reactive compounds (O_2 and CO) it is necessary to slightly modify the original expressions in order to avoid numerical problems and to facilitate convergence. By incorporating the parameter $\kappa = 1 \times 10^{-6}$ into Eqs. (24) and (25), the numerical problems are overcome without loosing accuracy on output results (Fig. 1). In addition, parameter κ corrects the reaction kinetics "to

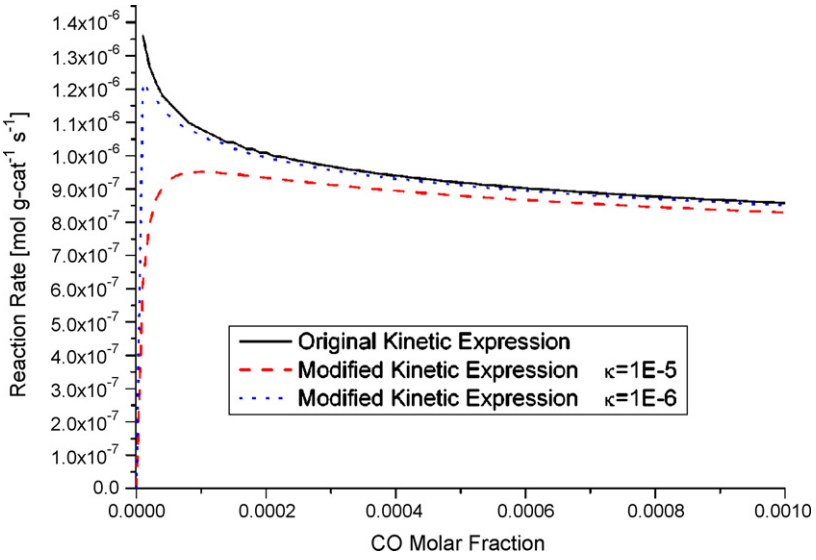

Fig. 1. Reaction rate comparison for different κ parameter values.

force" the reaction rates tending to zero when the reactant concentrations tend to zero. The kinetic expressions are

$$r_{CO} = 0.098000 \exp\left(-\frac{33092}{RT}\right)((P_{O_2}+\kappa)^{0.5} - \kappa^{0.5})\left(\frac{P_{CO}}{\kappa + P_{CO}^{1.1}}\right) \quad (24)$$

$$r_{H_2} = 0.005703 \exp\left(-\frac{18742}{RT}\right)((P_{O_2}+\kappa)^{0.5} - k^{0.5}) \quad (25)$$

$$r_{WGS} = 1.222778 \exp\left(-\frac{34104}{RT}\right)\left(P_{CO}P_{H_2O} - \frac{P_{H_2}P_{CO_2}}{K_{eq}}\right) \quad (26)$$

where

$$K_{eq} = \frac{P_{H_2}P_{CO_2}}{P_{CO}P_{H_2O}}$$

being

$$\ln(K_{eq}) = \frac{5693.5}{T} + 1.077 \times \log(T) + 5.44 \times 10^{-4}\,T - 1.125 \times 10^{-7}\,T^2 - \frac{49170}{T^2} - 13.148$$

3.5. Catalyst specifications

The catalyst particle has a density of 1.1 $g_{cat}\,cm^{-3}{}_{particle}$, with a Pt density of 0.0011 $g_{Pt}\,cm^{-3}{}_{active\ zone}$ [32], platinum is the active component and is considered uniformly distributed inside the particle; that is, the whole particle is assumed as "active zone". On the other hand, an egg-shell type catalyst particle with the same particle density but with an active catalyst density varying along the radio is considered (Fig. 2). The Pt density is equal to 0.00771 $g_{Pt}\,cm^{-3}{}_{active\ zone}$ in the "active zone" and zero in the "non-active zone". As an egg-shell type model with diffusion resistance becomes difficult to be optimized from a numerical point of view, the optimization model is based on a catalyst particle with uniform Pt distribution, without diffusion resistance. This model is an approximation to the egg-shell particle model considered above. This assumption is later verified in Section 4.

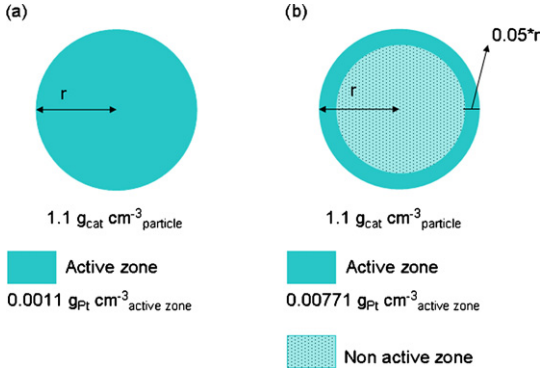

Fig. 2. Catalyst particle models used. (a) Catalyst particle model used for optimization; (b) egg-shell type catalyst particle model.

3.6. Optimization model

The optimization problem is formulated to obtain the optimal operating conditions and equipment size aiming at minimizing the total system volume. Following, the optimization problem is formulated; i.e. the objective function, decision variables and constraints are specified.

Objective function	Min (V_{total})
Decision variables	T^0, L_t, D_t, D_p, e_{ins}
Interior point constraints	
Catalyst temperature	$T_S^{Low} \le T_S^S \le T_S^{Up}$
External insulator temperature	$T_{ins} \le T_{Ins}^{UP}$
Final point constraints	
Admissible pressure drop	$(P_{in} - P_{out})/P_{in} \le 0.3$
CO molar fraction	$y_{CO} \le 1 \times 10^{-5}$ (10 ppm)
Design constraints	
Plug flow condition	$L_t/D_p > 50$; $D_t/D_p > 10$

As mentioned, it is intended to minimize the total volume of the system. In a conventional fixed-bed reactor, the total volume is computed considering the different reactor items such as the catalyst bed, reactor tube, insulating material, distribution heads and

entrance length with inert material, which determine the following individual volumes:

$$\text{reactor volume}: \quad V_{\text{reactor}} = \frac{(D_t + 2e_{\text{ins}})^2 \pi L_t}{4}$$

$$\text{inert material volume}: \quad V_{\text{inert material}} = \frac{20D_p(D_t + 2e_{\text{ins}})^2 \pi}{4}$$

$$\text{hemispherical heads volume}: \quad V_{\text{hemispherical heads}} = \frac{4(D_t + 2e_{\text{ins}}/2)^3 \pi}{3}$$

Then, the total volume is

$$V_{\text{total}} = V_{\text{reactor}} + V_{\text{hemispherical heads}} + V_{\text{inert material}}$$

The optimization problem determines the optimal reactor length (L_t), reactor diameter (D_t), catalyst particle diameter (D_p) and insulating material thickness (e_{ins}) that minimize the total system volume. For adiabatic operation case, the constraints corresponding to the insulating material temperature (T_{ins}) and insulation thickness are not included into the model as decision variables.

Due to the exothermic nature of the PrOx reaction, it is desirable to keep the reactor temperature within a certain operating range. An upper temperature bound is set for avoiding catalyst sintering. At low temperature, the reaction rate diminishes, the kinetic expression is not longer valid, and water condensation occurs. Then, it is necessary to impose a lower temperature bound. The reactor inlet temperature (T_f^0) is a decision variable, and its value results from the optimization problem.

Summarizing, molar flow of component i (F_i), fluid temperature (T_f) and pressure along the reactor bed (P) are calculated from differential Eqs. (5)–(7). Component concentration ($C_{S,i}^S$) and temperature (T_S^S) at the external catalyst surface are obtained from Eqs. (8) and (9). The resulting differential algebraic equations (DAEs) are implemented and solved using gPROMS (general process modeling system) [33]. gPROMS is a general purpose modeling, simulation and optimization system software. DAEs are essentially sets of ordinary differential equations (ODEs) where some of the variables are constrained by algebraic relations. Then, the resulting initial value DAE problem is integrated along the z axial direction. Backward differentiation formula (BDF) type method is the algorithm chosen in gPROMS for solving the differential equation system. Finally, the optimization algorithm being used is the single-shooting method, which is also available in the gPROMS environment.

4. Results and discussion

The reactor is designed considering the most probable conditions for the PrOx reaction in a small or medium scale ethanol processor. Molar flow rates and compositions at the PrOx reactor inlet considered for design correspond to the WGS exit conditions analyzed in a previous work [34]. The inlet molar flow rates per kW considered at the design stage are shown in Table 1. Apart from the main process stream, oxygen is fed to the reactor to perform the oxidation reaction. The results presented in this work correspond to an inlet O_2-to-CO molar flowrate ratio equal to 2.

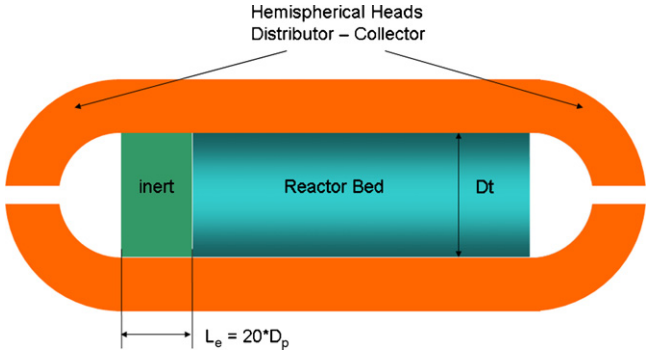

Fig. 3. System components included into the PrOx reactor model.

4.1. Design for 0.3% CO at the reactor inlet

Firstly, a system consisting on a single-stage reactor is considered. Four different objective functions are formulated, which differ in the number of system components included into the unit size computation. Specifically, Table 2 shows the results obtained for: (a) adiabatic reactor, (b) reactor + insulation, (c) reactor + insulation + distribution heads and finally, (d) same as case (c) but evaluating also an inert entrance length. A 0.3% CO composition at the reactor inlet is assumed for all cases.

In the adiabatic case, only the volume of the catalyst bed is considered. The "reactor + insulation material" system considers the reactor tube and insulation volumes. The insulating material used in the model consists of a layer of calcium silicate covered with a thin layer of aluminum. The insulating material conductivity is considered as a quadratic function of temperature according to the correlation $k(T) = 0.0264 + 7 \times 10^{-5}T + 6 \times 10^{-8}T^2$ taken from Industrial Insulation Group brochure [35].

A fully developed flow is considered at the reactor bed entrance. However, it should be taken into account that the flow into the fixed-bed reactor is generally achieved by means of a feed pipe and a distribution hood. These must therefore be constructed so that the fixed bed is uniformly traversed, and the gas residence time in each flow path of the fixed bed is the same. In order to evaluate the relative size of the components to achieve a uniform gas flow to the catalyst bed, the model is refined by including the reactor heads and an entrance with spherical inert particles. It has been found that an entrance length about $Le = 20D_p$ is enough to approach constant values independent of L for the gas flow parameters [29]. Finally, hemispherical distributor and collector are considered at the beginning and ending of the reactor (Fig. 3).

Table 2 lists the optimization results for the four cases analyzed to produce 10 kW for a 0.3% CO inlet concentration. Evidently, the

Table 1
Inlet PrOx reactor molar flow rates and compositions

Design	1% CO		0.7% CO		0.3% CO	
	Molar flow rate (mol h^{-1})	Molar fraction	Molar flow rate (mol h^{-1})	Molar fraction	Molar flow rate (mol h^{-1})	Molar fraction
CH_4	4.67	0.0563	4.67	0.0563	4.67	0.0563
H_2	41.97	0.5057	42.22	0.5087	42.55	0.5127
CO	0.83	0.0100	0.58	0.0070	0.25	0.0030
H_2O	20.59	0.2481	20.34	0.2451	20.01	0.2411
CO_2	14.94	0.1800	15.19	0.1830	15.52	0.1870

Table 2
Optimization results considering different objective functions

Design for 0.3% CO	Power target 10 kW			
	(a)	(b)	(c)	(d)
L_t (cm)	2.81	2.5*	9.37	8.25
D_t (cm)	6.19	6.74	3.71	4.08
D_p (cm)	0.05*	0.05*	0.19	0.10
e_{ais} (cm)	0	3.51	2.91	2.91
T_{in} (K)	528.0	522.0	511.4	507.6
T_{out} (K)	574.0	567.6	554.8	550.2
Bed volume (cm^3)	84.5 (100%)	89 (24%)	101 (09%)	108 (08%)
Insulation volume (cm^3)	–	282 (76%)	567 (51%)	527 (41%)
Heads volume (cm^3)	–	–	452 (40%)	508 (39%)
Inert entrance volume (cm^3)	–	–	–	154 (12%)
Total volume (cm^3)	84.5	372	1120	1297
Bed volume per kW produced ($cm^3\ kW^{-1}$)	8.5	8.9	10.13	10.79
Insulation volume per kW produced ($cm^3\ kW^{-1}$)	0	28.2	56.66	52.72
Heads volume per kW produced ($cm^3\ kW^{-1}$)	0	0	45.24	50.8
Entrance volume per kW produced ($cm^3\ kW^{-1}$)	0	0	0	15.4
Total volume per kW produced ($cm^3\ kW^{-1}$)	8.5	37.2	112.0	129.7

(a) Adiabatic reactor; (b) reactor + insulation; (c) reactor + insulation + heads; (d) reactor + insulation + heads + inert entrance; the asterisk shows that the variable reaches the minimum admitted value in the optimization process.

more detailed the model is, the better it represents the real system investigated. The adiabatic reactor model computes an optimal reactor diameter greater than its length, rendering a diameter-to-length ratio of 2.2. Then, the model is extended by adding insulation material. In this case, the catalytic bed volume increases 5.3% with respect to the previous model, and the diameter-to-length ratio increases to 2.7. It should be noted that the computed reactor length is at the lower bound value fixed. This is because the model tries to take advantage of the exothermic reaction which is developed inside the reactor along radial direction. The total system volume is 372 cm^3, of which 76% corresponds to the insulating material volume. If hemispherical heads – to favor an uniformly distributed flux – are incorporated into the model, the optimization results provide a different "qualitative" reactor geometry; specifically, in this case the optimal reactor length is greater than its diameter instead, rendering a diameter-to-length ratio of 0.4. The total system volume (1120 cm^3) increases tremendously with respect to the previous cases. The volume of the catalytic bed, insulating material and heads represent 9%, 51% and 40% of the total volume, respectively. Finally, an inert length entrance is also incorporated into the model for the same reason as reactor heads were considered. In this case, the diameter-to-length ratio is around 0.5. The optimal volume computed for the entrance length is 154 cm^3, which represents 12% of the total system volume. The total volume increases 16% with respect to the previous case. Based on these model-based results, the final reactor design is mainly governed by the presence of hemispherical heads.

Table 2 shows that the inlet reactor temperature T_{in} varies 20 K from model (a) – column 1 – to model (c) – column 4 – and that the temperature differences at the reactor outlet (T_{out}) and inlet (T_{in}) range between 42.6 K and 46 K for all analyzed cases. The small disagreement among models is because of the variation of the reaction heat with temperature and the heat loss to surroundings.

Finally, it can be observed that the optimal catalyst particle size is sensitive to the model being used. Certainly, the particle diameter computed for models (a) and (b) is at the lower bound value fixed (0.05 cm), and 0.19 and 0.10 cm for models (c) and (d), respectively. A lower bound for particle diameter of 0.05 cm was set for practical reasons. In order to compare optimization results with respect to other scenarios, Table 2 also lists the optimal volume values per kW of generated power.

4.2. Effect of the power generation level

Four design targets regarding the fuel cell power generation level are analyzed to achieve 10 ppm CO concentration at the reactor outlet: 1, 10, 25 and 50 kW. As above, process streams with CO compositions of 0.3%, 0.7% and 1% at the reactor inlet are assumed. The results obtained are listed in Table 3. The optimization problem allowed achieving a feasible design for each case that fulfills the imposed constraints. It should be noted that different system designs and arrangements are achieved depending on the desired power targets.

As mentioned, due to the exothermic nature of the involved reactions, a main difficulty in reactor design is to keep the operation temperature within the desired limits. If 1% CO level is specified at the reactor inlet, two units in-series (R1 and R2) are needed to achieve a CO concentration of 10 ppm at the reactor outlet for the four power generation targets being considered. That is, an arrangement of two units with intermediate cooling has to be considered for those scenarios. Figs. 4–6 show the relative volumes (in percentage) computed for the system components for all power design targets and inlet CO compositions being investigated. Since the reaction is highly exothermic, a large insulation volume is required. Heads and entrance lengths have an important contribution to the total volume of the system. That is necessary to achieve a uniform gas flow distribution pattern to the catalyst bed.

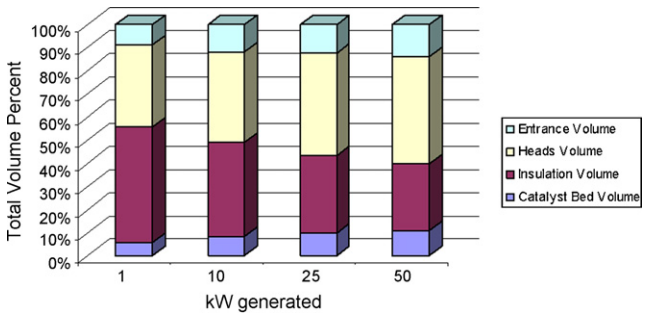

Fig. 4. Relative volumes of system components corresponding to four generation power targets for 0.3% CO molar fraction at the entrance.

Table 3
Optimization results for different design targets

	Reactor + Insulation + Headers + Entrance Length															
CO Inlet [%]	0.3				0.7				1							
CO Outlet [ppm]	10	10	10	10	10	10	10	10	10		10		10		10	
Power [kW]	1	10	25	50	1	10	25	50	1		10		25		50	
Amount of units	1	1	1	1	1	1	1	1	2		2		2		2	
Unit #	R1	R1	R1	R1	R1	R1	R1	R1	R1	R2	R1	R2	R1	R2	R1	R2
L_t [cm]	6.08	8.25	8.45	8.94	6.50	9.88	11.54	13.49	4.77	5.50	9.53	5.84	10.51	4.15	6.20	6.20
D_t [cm]	1.85	4.08	6.21	8.20	1.88	4.89	7.19	9.45	2.08	1.58	4.78	4.53	8.50	7.08	9.72	9.52
D_p [cm]	0.05	0.10	0.12	0.16	0.05	0.06	0.09	0.14	0.05	0.05	0.12	0.09	0.07	0.08	0.12	0.12
e_{ins} [cm]	1.97	2.91	3.32	3.69	2.56	3.36	3.71	3.98	2.06	2.43	2.76	3.24	3.85	2.34	3.97	4.00
T_{in} [K]	474.4	507.6	511.8	518.7	475.3	475.3	474.0	472.8	451.4	499.0	452.5	505.0	447.7	465.7	497.9	508.7
T_{out} [K]	516.8	550.2	555.3	562.4	571.8	573.9	573.5	572.7	519.9	568.6	531.9	567.8	574.3	485.7	570.2	572.2
Bed Vol. [cm^3]	16	108	256	472	18	186	469	946	16	11	171	94	596	163	460	441
Insul.Vol. [cm^3]	144	527	840	1232	232	860	1466	2265	128	168	623	462	1570	287	1059	1053
Heads Vol. [cm^3]	102	508	1111	1980	180	819	1633	2763	125	140	572	699	2226	852	2884	2816
Entrance Vol. [cm^3]	26	154	311	610	38	127	302	667	30	33	200	171	289	174	588	579
Total Vol. [cm^3]	288	1297	2518	4295	468	1992	3869	6641	651		2992		6157		9879	
Bed Vol./kW [cm^3 kW^{-1}]	16.35	10.79	10.24	9.44	18.04	18.56	18.74	18.92	16.21	10.78	17.10	9.41	23.86	6.54	9.20	8.83
Insul Vol./kW [cm^3 kW^{-1}]	143.84	52.72	33.60	24.64	232.11	86.04	58.64	45.31	127.80	168.37	62.31	46.19	62.80	11.50	21.17	21.07
Heads Vol./kW [cm^3 kW^{-1}]	101.63	50.80	44.44	39.60	179.59	81.94	65.31	55.26	124.79	139.85	57.22	69.88	89.04	34.06	57.68	56.32
Entrance Vol./kW [cm^3 kW^{-1}]	26.33	15.40	12.45	12.20	38.48	12.70	12.07	13.33	30.19	32.57	20.00	17.14	11.54	6.95	11.76	11.57
Total Vol./kW [cm^3 kW^{-1}]	288	130	101	86	468	199	155	133	651		299		246		198	

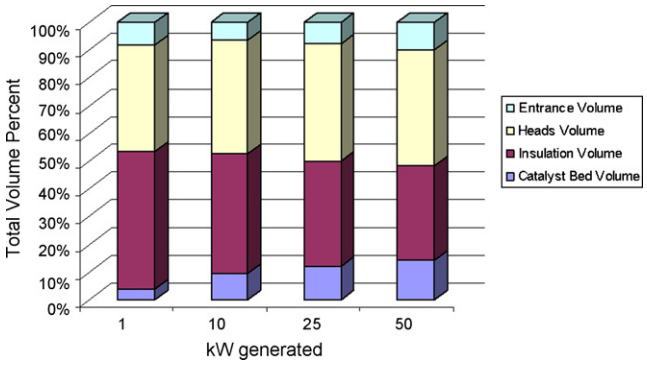

Fig. 5. Relative volumes of system components corresponding to four generation power targets for 0.7% CO molar fraction at the entrance.

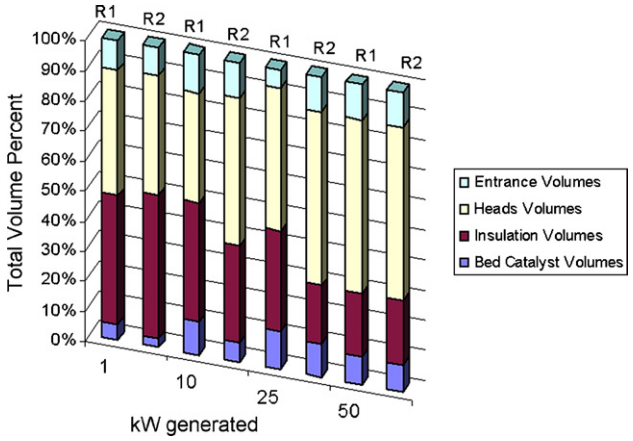

Fig. 6. Relative volumes of system components corresponding to four generation power targets for 1% CO molar fraction at the entrance. Two reaction units in-series (R1 and R2).

4.3. Reactor simulation

Following, a comparison of simulated profiles obtained with different reactor models is presented and discussed. In order to verify feasibility of the optimal design obtained with the methodology proposed using the one-dimensional heterogeneous model without intra-particle gradients, which is intended to approximate the egg-shell catalyst behavior, simulation runs were then conducted based on different reactor models. The simulations results correspond to the scenario with an inlet CO concentration of 0.7% and a flow rate equivalent to generate 10 kW of power (see Table 3).

The reactor models being compared are: (i) the mentioned model used for optimal design, named 1D-HtEx; (ii) a one-dimension heterogeneous model with intra-particle gradients, named 1D-HtInt; finally, (iii) a two-dimensional pseudohomogenous model, named 2D-PH. Based on the 1D-HtInt model, two different situations regarding the catalyst distribution were addressed: (a) uniform distribution of the catalyst activity in the particle with a Pt density equal to 0.0011 $g_{Pt}\,cm^{-3}{}_{cat}$, named 1D-HtIntU; (b) an "egg-shell"-type model, named 1D-HtIntES, where the catalyst activity is concentrated in an "active outer zone" corresponding to around 5% of the particle radius with a Pt density equal to 0.00771 $g_{Pt}\,cm^{-3}{}_{active\ zone}$ [32].

The CO molar fraction profiles established along the reactor are depicted in Fig. 7, and the composition profiles inside the catalyst particle are shown in Fig. 8. It can be observed that the conversion values predicted by the 1D-HtEx model and the 1D-HtIntES model are similar. Meanwhile the 2D-PH model and 1D-HtIntU model predict higher and lower conversion values than the 1D-HtEx model, respectively.

This behavior is due to the fact that the average temperature predicted by the 2D-PH model is higher (Fig. 9), which increases the reaction rate, thus requiring less volume to achieve the desired target. Although the conversion predicted by the 1D-HtIntU model

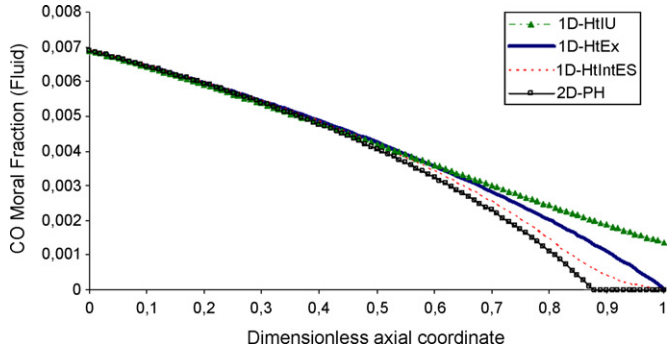

Fig. 7. CO molar fraction profiles along the reactor length.

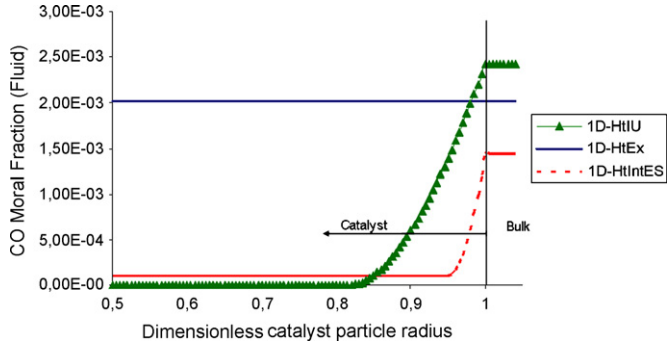

Fig. 8. CO molar fraction profiles inside the catalyst particle.

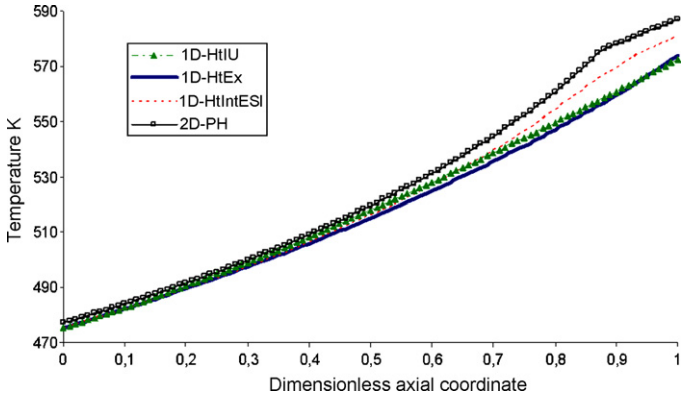

Fig. 9. Temperature profiles predicted by the different models considered.

is higher at the first sections of the reactor, which is indicated through the higher temperature profile, the diffusion phenomena compete with the reaction ones at the last sections of the unit, thus decreasing the catalyst effectiveness and, consequently, lowering the conversion values.

According to the aims set out in this paper, the results of the models comparison allow confirming the application of the 1D-HtEx model for optimal reactor design when considering a catalyst with non-uniformly distributed activity (egg-shell type catalyst). Nevertheless, the higher average temperature predicted by the 2D-PH model suggests further consideration of a two-dimensional heterogeneous model. In addition, in future works, the O_2-to-CO molar ratio will be considered as a decision variable, as well as the possibility of oxygen and/or water flow distribution along the reaction zone instead of a unique feed point.

5. Conclusions

As regards the used methodology, the results of the present work reflect clearly the advantages of applying mathematical programming techniques to optimize both design and operation conditions of the PrOx reactor, which is subjected to several trade-offs involving operative, construction, technological and efficiency constraints. Indeed, the proposed methodology was applied to different scenarios and targets, showing satisfactory robustness and flexibility.

The heterogeneous reactor model being used allows computing the optimal reactor length and diameter, optimal catalyst particle diameter, optimal insulating material thickness, as well as the optimal inlet temperature of the stream to operate the system in a pseudo-adiabatic mode.

Under the investigated scenarios, and depending on the CO content to be treated, more than one catalytic bed may be required. Indeed, it is possible to successfully process a stream with an inlet CO concentration of 0.3% or 0.7% in a unique stage, maintaining restrictions on the bed temperature. However, for higher CO concentration, 1% for instance, two stages in-series with intermediate cooling are needed.

The model being used predicts a behavior similar to a catalyst with a non-uniformly distributed activity ("egg-shell"). Nevertheless, the 2D-PH model and 1D-HtIntU model predict higher and lower conversions with respect to the ones corresponding to the design targets.

Although the presented optimization results strongly depend on the particular catalyst and on the considered inlet/outlet specifications, the proposed methodology and the obtained preliminary results can assist in designing, optimizing and controlling the global process, i.e. commercial fuel processors for producing hydrogen for fuel cells applications.

Acknowledgments

Financial support from the Consejo Nacional de Investigaciones Científicas y Técnicas (CONICET), Agencia Nacional para la Promoción de la Ciencia y la Tecnología (ANPCyT) and the Universidad Nacional del Litoral of Argentina is acknowledged.

References

[1] L.F. Brown, Int. J. Hydrogen Energy 26 (2001) 381–397.
[2] M. Krumpelt, T.R. Krause, J.D. Carter, J.P. Kopasz, S. Ahmed, Catal. Today 77 (2002) 3–16.
[3] P.C. Hulteberg, J.G.M. Brandin, F.A. Silversand, M. Lundberg, Int. J. Hydrogen Energy 30 (2005) 1235–1242.
[4] M. Echigo, T. Tabata, Catal. Today 90 (2004) 269–275.
[5] Y. Choi, H.G. Stenger, J. Power Sources 129 (2004) 246–254.
[6] O. Korotkikh, R. Farrauto, Catal. Today 62 (2000) 249–254.
[7] M. Echigo, T. Tabata, Appl. Catal. A 251 (2003) 157–166.
[8] M.M. Schubert, M.J. Kahlich, H.A. Gasteiger, R.J. Behm, J. Power Sources 84 (1999) 175–182.
[9] E.J. Bissett, S.H. Oh, R.M. Sinkevitch, Chem. Eng. Sci. 60 (2005) 4709–4721.
[10] M.J. Kahlich, H.A. Gasteiger, R.J. Behm, J. Catal. 182 (1999) 430–440.
[11] S.H. Oh, R.M. Sinkevitch, J. Catal. 142 (1993) 254–262.
[12] M. Echigo, N. Shinke, S. Takami, S. Higashiguchi, K. Hirai, T. Tabata, Catal. Today 84 (2003) 209–215.
[13] G. Sedmak, S. Hocevar, J. Levec, J. Catal. 213 (2003) 135–150.
[14] G. Zhou, Y. Jiang, H. Xie, F. Qiu, Chem. Eng. J. 109 (2005) 141–145.
[15] F. Mariño, C. Descorme, D. Duprez, Appl. Catal. B 58 (2005) 175–183.
[16] X. Ouyang, R.S. Besser, J. Power Sources 141 (2005) 39–46.
[17] S. Srinivas, A. Dhingra, H. Im, E. Gulari, Appl. Catal. A 274 (2004) 285–293.
[18] E.J. Bissett, S.H. Oh, Chem. Eng. Sci. 60 (2005) 4722–4735.
[19] I. Toyoshima, G.A. Somorjai, Catal. Rev. Sci. Eng. 19 (1979) 105–159.
[20] S.H. Lee, J. Han, K.-Y. Lee, J. Power Sources 109 (2002) 394–402.
[21] J.M. Zalc, D.G. Loffler, J. Power Sources 111 (2002) 58–64.
[22] C.D. Dudfield, R. Chen, P.L. Adcock, J. Power Sources 85 (2000) 237–244.
[23] C.D. Dudfield, R. Chen, P.L. Adcock, Int. J. Hydrogen Energy 26 (2001) 763–775.

[24] G.F. Froment, K.B. Bischoff, Chemical Reactor Analysis and Design, 2nd ed., Wiley, New York, 1990.
[25] S. Hwang, R. Smith, Chem. Eng. Sci. 59 (2004) 4229–4243.
[26] J. Carberry, A. Varma, Chemical Reaction and Reactor Engineering, Marcel Dekker, New York, USA, 1987.
[27] R.C. Reid, J.M. Prausnitz, B.E. Poling, The Properties of Gases and Liquids, 4th ed., McGraw-Hill, New York, 1987.
[28] R.H. Perry, C.H. Chilton, Chemical Engineering Handbook, 5th ed., McGraw-Hill, New York, 1973.
[29] I. Ziolkowska, D. Ziolkowski, Chem. Eng. Process. 44 (2005) 1167–1180.
[30] C.N. Satterfield, Mass Transfer in Heterogeneous Catalysis, MIT Press, Cambridge, 1970.
[31] A.R. Koenig, Chem. Eng. (New York) 87 (1980) 125–128.
[32] D.H. Kim, M.S. Lim, Appl. Catal. A 224 (2002) 27–38.
[33] gPROMS, Introductory User Guide (Release 2.3), Process Systems Enterprise Ltd., 2004.
[34] J.A. Francesconi, M.C. Mussati, P.A. Aguirre, J. Power Sources 173 (2007) 467–477.
[35] Industrial Insulation Group (http://www.iig-llc.com).